Subsurface detections by SHAllow RADar (SHARAD) on MARS

S. K. Mishra and Rajiv R. Bharti

Physical Research Laboratory, Ahmedabad 380009, India
E-mail: sanjaym@prl.res.in

Dr. Sanjay K. Mishra is a PRL Physicist, having diverse research experience at various levels. His research interest is interdisciplinary plasma physics, including space and dusty (complex) plasma, laser-plasma interaction, sheath physics, and electronic transport processes. He is Young Associate of IASc, Bangalore, and recipient of the IPA Buti Foundation Award 2018.

Rajiv R. Bharti is a Scientist in the Planetary Sciences Division, PRL. His research area is the study of surface and subsurface of Mars using remote sensing data of various missions. Currently, he is working on the data of SHARAD to investigate the geophysical properties of Martian subsurface.

Abstract

Orbiter sounding radars have been proven a vital tool in deriving the stratigraphic and geological information of the planetary bodies in the planetary exploration. SHAllow RADar (SHARAD) onboard Mars Reconnaissance Orbiter (MRO) spacecraft, orbiting Mars, is considered one of the very successful sounding radar mission detecting the subsurface interfaces beneath the Martian surface. The prime objective of such sounders is the search for water ice and aquifers within the Martian surface. Due to high-frequency operation mode, SHARAD has detected the ice layers around the polar caps and mid-latitude regions of Mars within few 100 meters beneath the top surface. In this article, we briefly present the concept, operation, and science objectives of SHARAD, alongwith a plausible approach to derive the dielectric properties of the subsurface materials from the SHARAD observations.

Introduction

Planetary exploration via in situ measurements and orbiter remote sensing has brought out significant information that has advanced our understanding of the Martian surface and climate history [1-3]. Particularly, due to global coverage of the planet, the orbiter radars are proven important instruments in identifying the adequate habitable zone for the forthcoming robotic and human explorations [3]. The search for the quest of subsurface water deposits has been the prime focus of the campaigns so far to the Mars, and the low-frequency orbiter radars with high penetration capabilities have been successful in depicting such regions [4]. For instance, the Mars Advanced Radar for Subsurface and Ionosphere Sounding (MARSIS), in 2012, first depicted the evidence of lower-density material that fills the northern basin, indirect evidence of an ancient northern ocean [5]. The discovery of the first water reservoir in the form of the subglacial lake of 20 km extension on Mars below the southern polar ice cap [6] has been another notable breakthrough by MARSIS. MARSIS operates at frequencies between 1.8 and 5.0 MHz in subsurface sounding mode, with a 1 MHz bandwidth, that corresponds to the vertical resolution of 150 m – with this configuration, MARSIS was able to detect the subsurface soundings from the ~1 – 5 km vertical extent, however, due to the coarse resolution, the instrument was not compatible with providing the stratigraphy description within the first km below surface [4]. This is where the requirement of another device with the lower vertical resolution was realized, and the SHAllow RADar (SHARAD) instrument was conceptualized [7].

SHARAD is the instrument from the Italian Space Agency (ASI) operating at center frequency of 20 MHz (with 10 MHz bandwidth) and 10 – 20 m vertical resolution – SHARAD is flown with NASA's Mars Reconnaissance Orbiter (MRO) in 2005 [8]. The operational orbit of MRO spacecraft is nearly polar, quasi-circular, and sun-synchronous – it secures optimal illumination conditions for optical instruments. The science objective of SHARAD is to map the dielectric interfaces to a few hundred meters depth on selected sites, and interpret the radar data in terms of the occurrence and distribution of the expected materials within the subsurface layers – this includes the water, ice, soil, and rocky materials. The observations from SHARAD are anticipated to complement the MARSIS findings by refining the near-surface composition, stratigraphy, and structure for the first few 100's m beneath the surface – refined structures of the internal layers of the polar caps were of prime interest [8]. Among numerous science

results, the detection of layered ice deposits around north pole of Mars [9], and the underground ice (i.e., equivalent to the volume of the water in Lake Superior, North America) in the Utopia Planitia region of Mars [10], are a couple of outstanding discoveries from SHARAD.

In this article, we particularly focus on the SHARAD operation and describe the inherent physics principle, analysis method, scientific objectives, and significance. For a detailed description of the technical and scientific challenges in the instrument design and development, data acquisition and processing, and overall instrument operation, the readers are referred to Ref. [7-8], and the references therein.

Operational principle and specifications

The working principle of the SHARAD instrument is quite simple and is based on the radio wave transmission through a medium. Due to large wavelength, the radio wave possesses the capability to penetrate the surface, which is frequently used in the ground-penetrating radar systems for archeological surveys and terrestrial applications. As radio wave falls on the target, a large fraction of energy reflected from the surface, while it partially transmits into the surface depending on the dielectric properties of the medium. The transmitted wave may exhibit further reflections as signal encounters dielectric discontinuities – these signals, which carry the dielectric info of the geological layers in terms of power, are gathered by antenna receiver for further data processing. Intuitively, the subsurface reflections can be much weaker than those from the surface because of medium losses. SHARAD produces data for reflections from surface and subsurface layers in terms of twt delay, and respective power – this graphical representation is termed as 'radargram' [8] and infers the dielectric contrast encountered by a signal in its transmission. Such discontinuity on Mars could arise from many combinations of surface and subsurface materials. This may include the contacts of sediments with basaltic cover, ice with solid rock, icy porous with porous/ solid rocks, volcanic flows, etc. – these stratigraphic features deduce the physical evolution of the Martian surface and climate [8].

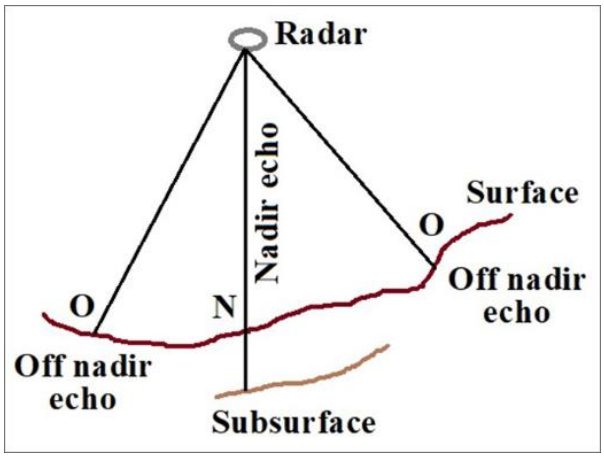

Figure 1*: Schematic of the clutter generation through off-nadir surface echoes.*

Moreover, the operation of orbiter radars from significantly large altitudes, and directivity constraints, generate clutter in the form of off-nadir echoes alongwith the nadir surface and subsurface echoes [8]. As shown in Figure 1, the radar receives reflections from the off-nadir locations as well, in addition to nadir echoes. Depending on the topography and roughness of the target surface, the off-nadir clutter echoes may be significant to disguise it as an actual subsurface echo. In order to overcome this, the idea is to reduce the radar footprint. In this course, SHARAD works on the principle of Synthetic Aperture Radar (SAR) to achieve a fine along-track resolution [4] – depending on the orbiter location and region of interest on the Mars, SHARAD may achieve the horizontal resolution of 0.3 – 3 km along and 3 – 6 km across the track [8]. This technique, however, reduces the footprint of antenna radar, but could not completely diminish the effect of clutter originated from nearby off-nadir irregularities. This can be overcome by simulating the Mars surface and irregularities at the scale of SHARAD interest – Mars Orbiter Laser Altimeter (MOLA) [11] topography data is used to construe the off-nadir echoes and delineate the adequate subsurface echoes from SHARAD radargram. With this approach, one can distinguish between the surface and subsurface signals. A complete description of clutter mitigation can be found in Refs. [11-12].

Table* 1: SHARAD parameters*

Parameter	Magnitude
Frequency band	15 – 25 MHz
Mean frequency	20 MHz
Vertical resolution	15 m (in a vacuum)
Penetration depth	0.1 – 1 km
Horizontal resolution	0.1 – 3 km (along track) 3 – 6 km (across track)
Peak signal power	10 W

Another concern is the temporal resolution of the signal. To optimize the instrument performance, it should be equivalent to the vertical space resolution (~ 15 m) – in terms of two-way time (twt) delay. This is equal to 100 ns or the bandwidth of 10 MHz [8]. To achieve such resolution, a linear chirped-pulse has been opted as the radar transmission signal. The nominal physical parameters for SHARAD [8] are listed in Table 1.

Subsurface detection

With the help of an example, we show the detection of true subsurface echoes. As an illustration, consider the SHARAD track over an LDA (lobate debris apron) structure [13] located at coordinates (46.12N, 28.15E) around northern-mid latitude Deuteronilus Mensae region on Mars – this area is shown in the bottom panel of Figure 2, with radar track (yellow line). The LDAs are the geological features on Mars, comprising of piles of rock debris with a convex topography, connected from cliffs with a gentle slope. LDA's are considered the signatures of the phase of glacial activities on Mars – the geomorphic and topographic studies of LDAs have suggested their formation by downflow of ice-debris mix away from the plateau during the past ~ (1Ga – 100Ma). The geomorphic studies and limited occurrence give evidence of accumulation of km thick ice at a certain depth in northern and southern mid-latitudes of Mars. Using SHARAD data, Plaut et al. [14] have shown the typical

rate of decrease of ~2 dB/μs for the two-way echo attenuation for a real dielectric constant of 3 (i.e., nearly pure water ice).

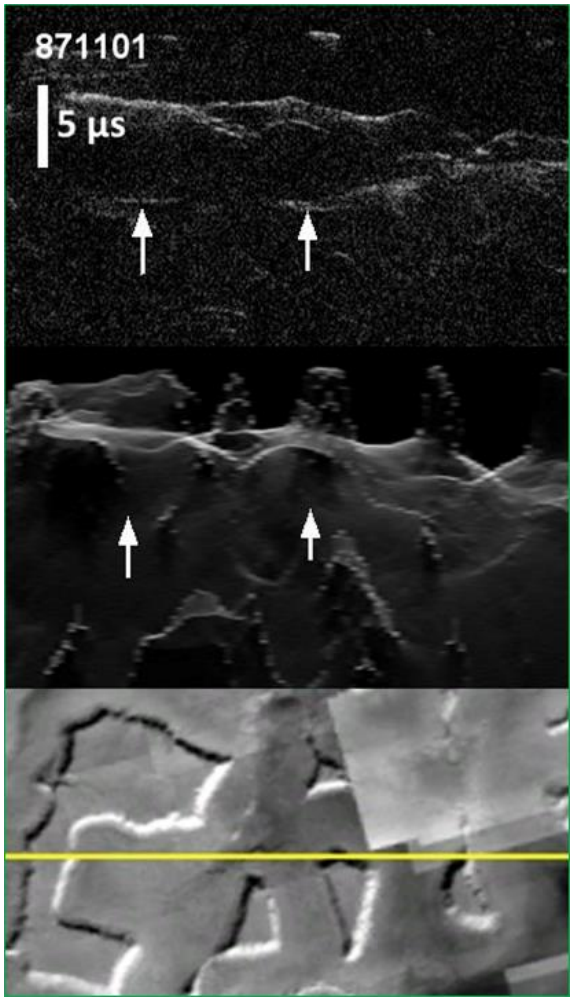

Figure 2*: Subsurface reflection: The top panel image refers to SHARAD radargram in terms of twt delay for track no.* 871101. *Middle panel image is the simulated cluttergram displaying off-nadir echoes. The bottom panel refers to the daytime IR THEMIS* (*Thermal emission imaging system*) *image of LDA.*

The subsurface radar sounding of the apron extent indicates that these deposits are composed mainly of water ice, which is preserved at shallow depths beneath the LDAs [14].

The top panel of Figure 2 illustrates the reflection echoes received by SHARAD in the form of the radargram – this combines the information of reflected signals from the surface and subsurface layers along the track in the form of twt delay and signal intensity (in dB units). The middle panel of Figure 2 refers to the cluttergram generated using MOLA topography data for the same location. Comparing the two figures (top and middle panels), one may clearly distinguish the true subsurface reflections from those of off-nadir echoes; the subsurface features have been depicted by white arrows in the SHARAD radargram. To interpret the SHARAD data for mapping the distribution of the subsurface reflections and for exporting the relative subsurface reflection intensity or signal power, commercially available seismic software has been used. The sharp-intense white line along the track refers to the magnitude of power (in dB) received by radar receiver after reflection from the surface. Just below, the faint white lines of relatively lower intensity correspond to the reflected power (in dB) from the subsurface layers. Using these data set, the power associated with surface and subsurface reflections can be represented as a function of twt delay – this information we use to determine the dielectric properties of the subsurface material that we discuss next.

Dielectric permittivity of the subsurface material

Radar echoes/ signals received after reflection/ scattering describes the characteristic dielectric features of the material of layers and sublayers [3]. As an electromagnetic (em) radio wave interacts with the surface, it exhibits partial reflection, scattering and transmittance. The transmitted wave propagates further within the surface and again exhibits partial reflection/ transmittance at any other dielectric discontinuity beneath. In this process, the waves also suffer the attenuation and phase change on account of its absorption within the medium. This process continues until the wave diminishes completely. These partial reflections from surface and sub-surfaces are usually recorded by the radar in terms of the power at different (two way) time delays, which eventually carries cumulative effects of the dielectric features and sublayer widths.

To extract this information from the recorded (SHARAD) data, an inversion approach [15] of the reflection/ scattering analysis is usually adopted, and estimates are made on the basis of backward calculations. We herewith briefly describe the reflection model based on the linear theory of em wave propagation [16]; as SHARAD experiment is operating with low power signals, linear calculations are well applicable. The first reflection occurs as the signal wave interacts with vacuum – top surface interface. To model the radar observations, we consider the physical picture where the subsurface material is considered sandwiched between the successive flow deposits. A schematic of this physical model is shown in Figure 3. In addition to top surface layer, we consider two main interfaces viz. (1) top surface layer – subsurface, and (2) subsurface – base layer; both the interfaces are considered planar, and the layers are assumed to be homogeneous and nondispersive. The subsurface layer is further considered as a low-loss medium with the intensity attenuation coefficient (α). Considering the large distant radar observations, the planar wavefront with a normal incidence of the wave has been modeled.

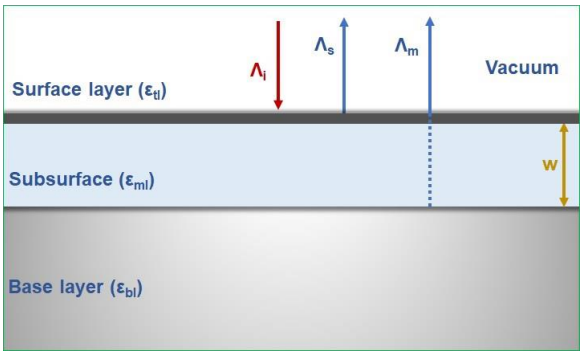

Figure 3*: A schematic of the physical model considered for the calculation of the power reflectance* (*Eq.*5).

Following Fresnel's formulation, the power reflected from the top surface into the vacuum (Λ_s) and the power transmitted (Λ_T) into the surface, maybe given in terms of the incident power (Λ_i) as

$$\Lambda_s = \gamma_{tl}^2 \Lambda_i \;\&\; \Lambda_T = (1-\gamma_{tl}^2)\Lambda_i, \qquad (1\ \&\ 2)$$

where $\gamma_{tl} = (k_o - k_{tl})/(k_o + k_{tl})$, $k_{tl} = k_o \varepsilon_{tl}^{1/2}$, k_o (= $2\pi\nu/c$ = $2\pi/\lambda_o$), k_{tl} and ε_{tl} stand for the wavenumber and dielectric constant of the top surface layer, ν, λ_o and c correspond to the mean frequency (20 MHz), wavelength (15 m) and light speed (i.e., 300 $m/\mu s$) in the free space for SHARAD operation.

The wave transmitted through the top layer (Λ_T) acts as an incident wave for the 1st (i.e., surface–subsurface) interface. In evaluating the reflectance from the subsurface layer, we take account of the propagating solution of the wave equation in the constituent (i.e., surface – subsurface – base layer) region. By matching the continuity of the wave solutions and their derivatives at layer interfaces (1st & 2nd), the coefficient of the wave amplitude reflection and transmission may be obtained as a function of the medium variables [2]. With little algebra, the reflection coefficient at 1st interface may be expressed as

$$\gamma_{ml} = \frac{(k_{tl}-k_{ml})(k_{ml}+k_{bl}) + (k_{ml}-k_{bl})(k_{tl}+k_{ml})e^{-2ik_{ml}w}}{(k_{tl}+k_{ml})(k_{ml}+k_{bl}) + (k_{ml}-k_{bl})(k_{tl}-k_{ml})e^{-2ik_{ml}w}}, \qquad (3)$$

here $k_{ml} = k_o \varepsilon_{ml}^{1/2}$ and $k_{bl} = k_o \varepsilon_{bl}^{1/2}$ refer to the wave vectors associated with the unknown (middle) subsurface layer (k_{ml}) and the base layer (k_{bl}). The optimum value of γ_{ml} corresponds to $k_{ml}w = \pi/2$, as $\gamma_{ml}^{opt} = (k_{tl}k_{bl} - k_{ml}^2)/(k_{tl}k_{bl} + k_{ml}^2)$. Moreover, for $k_{bl} = k_{tl}$, Eq.3 reduces to a simpler form, viz.,

$$\gamma_{ml} = \frac{(k_{tl}^2 - k_{ml}^2)[1 - exp(-2ik_{ml}w)]}{(k_{tl}+k_{ml})^2 - (k_{tl}-k_{ml})^2 exp(-2ik_{ml}w)}. \qquad (4)$$

It should be noted that for known k_{tl} and k_{ml}, γ_{ml} shows an oscillatory dependence on $k_{ml}w$ and take a value between 0 to optimum depending on subsurface width w. The real part becomes zero for $w = n\lambda_{ml}/2$ while takes maximum value for subsurface thickness $w = (2n + 1)\,\lambda_{ml}/4$, where n refers an integer, and λ_{ml} is the signal wavelength within the subsurface medium. As a simplification, let consider a linear attenuation of the wave within medium. It modifies the expression for power by a factor of $exp(-2\alpha w)$; here, $2w$ infers twt delay and equals ~ $(c\Delta\tau/\varepsilon_{ml}^{1/2})$. Thus, net em signal power approaching the radar in the after reflection may be expressed as

$$\Lambda_m = (\gamma_{ml}^2 e^{-2\alpha w})\Lambda_T = (1-\gamma_{tl}^2)^2 \gamma_{ml}^2 e^{-2\alpha w}\Lambda_i. \qquad (4)$$

Using Eq.1 and Eq.4, the ratio of the powers reflected from the surface and sub-surface layers may thus be expressed as

$$(\Lambda_m/\Lambda_s) = (1-\gamma_{tl}^2)^2(\gamma_{ml}^2/\gamma_{tl}^2)exp(-2\alpha w). \qquad (5)$$

The power reflectance (Λ_m/Λ_s) derived in Eq.5 is, in fact, an outcome of SHARAD data in the form of radargram, which illustrates the relationship between the power reflected along-track and round-trip time (twt) delay – from this, the ratio of reflected signal powers from surface and sub-surface, may be calculated as a function of time delay ($\Delta\tau$). The value of (Λ_m/Λ_s) at any given location may be used to obtain the subsurface dielectric constant (ε_{ml}) by solving Eq.5 for the known ε_{tl}. This model can be implemented with the measurements of (Λ_m/Λ_s) to constrain the possible values of ε_{ml}. For dry materials, the dielectric permittivity is directly correlated with density – this empirical relationship may be presented as [17]

$$\varepsilon_{ml} = 1.96^{\rho}, \qquad (6)$$

where ρ is the material density in gcm^{-3}.

Table 2: *SHARAD subsurface detections and corresponding dielectric properties*

Location on Mars	Dielectric Constant	Loss Tangent	Slope DB/μs	Material
NW Ascraeus [18]	7.6 ± 2.3	0.006	-3.3	Dense Low Ti Basalt
Ascraeus Mons (Northern flow)[19]	6.2-17.3	0.01-0.03	-7.9	Dense Low Ti Basalt
Ascraeus Mons (Southern flow)[19]	7.0-14.0	0.01-0.03	-----	Terrestrial/ Lunar Basalt
Amazonis Plantia [20]	----	0.009	-4.98	Moderate density Sediments
LDA's [9]	~3.0	----	-2.0	Water Ice

Moreover, in the realistic scenario, the interfaces may not be exactly planar, and the width of the subsurface (and hence the two-way time delay) may vary along the track. Usually, the SHARAD data is graphically presented as a relation between the power loss ($\Lambda_m - \Lambda_s$) in dB and respective two-way time delay $\Delta\tau$ – the departure of the data from flatness, $\Delta\tau$ is a signature of the signal attenuation in the medium. Noted, the power reflectance (Λ_m/Λ_s) in dB refers to the difference of the power reflected (in units of dB) from the two successive interfaces. In this context, rewriting Eq.5 in terms of power loss in dB and $\Delta\tau$ can be expressed as

$$\left(\frac{\Lambda_m}{\Lambda_s}\right)_{dB} = -\left(\frac{10\alpha c}{\varepsilon_{ml}^{1/2} ln10}\right)\Delta\tau + 10log\left(\frac{(1-\gamma_{tl}^2)^2\gamma_{ml}^2}{\gamma_{tl}^2}\right). \qquad (7)$$

In view of Eq.5, an empirical linear fit between power loss (Λ_m/Λ_s) in dB and $\Delta\tau$ through SHARAD data may provide a notion about the magnitude of the absorption coefficient. For instance, the gradient of this linear relation refers to the loss rate of the subsurface material in the units of dB/μs. Another dielectric parameter that can be derived from the SHARAD data is the loss tangent. This physical quantity, by definition, represents the ratio of imaginary and real parts of the complex dielectric constant of the subsurface material; physically, it represents the power loss of the em radio wave as it traverses through the medium. Following Campbell et al. [20], the loss tangent consistent with the subsurface can be expressed as,

$$tan\delta = \left[\left[2[\lambda_o(lnL)/4\pi c\Delta\tau]^2 + 1\right]^2 - 1\right]^{1/2}, \qquad (8)$$

where L is the power loss per unit of time $\Delta\tau$.

For the sake of completeness and secure a notion of the subsurface characteristics, the dielectric constant and loss tangent of the SHARAD identified subsurface material on Mars are listed in Table 2; the data has been depicted from the various literature [9, 18-20].

Analytical illustrations

Here we present a few calculations based on the analytical expression derived in the last section. The expression for the power reflectance (Eq.5) suggests that its magnitude depends on the dielectric constants of constituent layers (ε), attenuation factor (α), and width of the sandwiched subsurface layer (w). The basalt is prominent material and commonly dispersed on the Martian surface; for calculations, the dielectric constant of the top surface may be taken as $\varepsilon_{tl} = 10$. Further, considering the fact that the basaltic lava flow has been the dominant process in stratigraphy evolution [18], we assume $\varepsilon_{tl} \approx \varepsilon_{bl} = 10$ in present calculations. Following the SHARAD detection of low-density subsurface deposits [20] around the region of Amazonis Planitia, the power loss between interfaces varies in the range (-17 dB to -5 dB) and corresponds to $(\Lambda_m / \Lambda_s) \sim 0.02 – 0.3$; higher the power reflectance corresponds to a significant contrast between the surface and subsurface materials. In other work by Carter et al. [19], high dielectric basaltic interfaces are detected beneath lava flow fields northwest of Ascraeus Mons. In this case, the power loss refers to a range (–90 dB to –75 dB) and corresponds to $\Lambda_m/\Lambda_s \sim 10^{-9}$ to $10^{-7.5}$; this infers weaker dielectric contrast between the surface and subsurface materials. Through SHARAD literature [8-15, 18-20], we note a significant variation in (Λ_m / Λ_s) values, and wide diversity in the subsurface deposits – we consider this (Λ_m / Λ_s) range as reference for our calculations.

In order to include the influence of the wave attenuation, we consider two cases with decay rates 0 (lossless medium), and 5 dB/μs (low-density materials, [18]) in the calculations. With these known parameters, Eq.5 is used to obtain a plausible parametric space between ε_{ml} and w, illustrating the power ratio (Λ_m / Λ_s) – this has been shown in Figure 4. This relation can be used to envisage the suitable range of the subsurface dielectric constant (ε_{ml}) and subsequent thickness (w) for given (Λ_m / Λ_s). Figure 4 indicates that depending on w, the subsurface dielectric constant may vary over a wide range, and multiple such combinations (ε_{ml}, w) are plausible for a given value of (Λ_m / Λ_s); this behavior is in conformance with the analytical prediction of Eq.4. The power reflectance is noticed large for the low dielectric values. It is also noticed that the inclusion of finite attenuation leads the solution to a lower dielectric permittivity value in comparison to a lossless medium for a given (Λ_m / Λ_s). This suggests that the dielectric and attenuation effects on the wave propagation and the signal power transmission are complementary.

In the context of SHARAD, for the known values of (Λ_m / Λ_s) and decay rate from the SHARAD data analysis, these variants derived in Figure 4 can be utilized to depict the plausible range of the dielectric constant, and hence the density (Eq.6) of the subsurface material. As depicted in

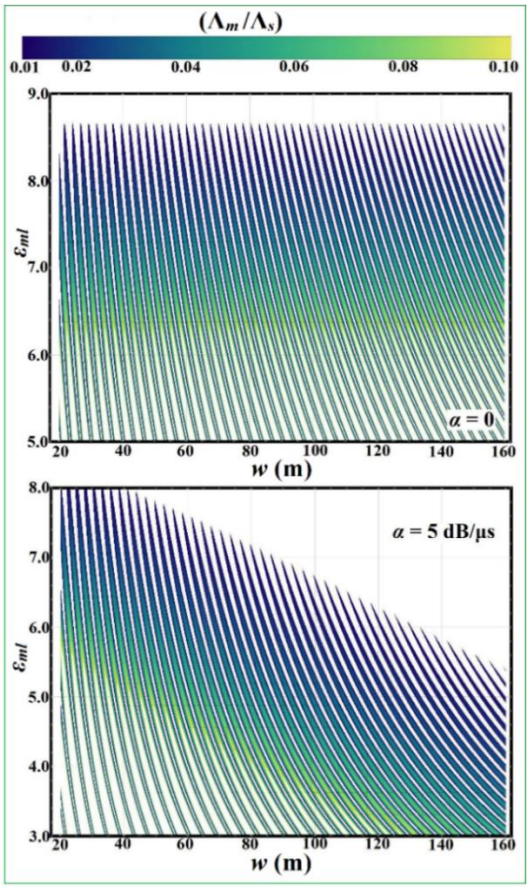

Figure 4: *Density plot: Estimate of the dielectric constant of the subsurface material ε_{ml} as a function of layer thickness w using Eq.5. The computations correspond to v = 20 MHz and $\varepsilon_{tl} = \varepsilon_{bl} = 10.0$; the top and bottom panels refer to the lossless medium and decay rate of 5dB/μs, respectively, while the color bar represents the magnitude of* (Λ_m / Λ_s).

Table 2, the large dielectric permittivity values correspond to the high-density basaltic subsurface deposits, while the moderate dielectric constant values may correspond to the subsurface deposits of low-density material. As depicted, depending on the subsurface thickness, the reflectance may take an optimum value – this may provide the best possible scenario of efficient detection of the subsurface echoes. In Figure 5, we have derived the dielectric permittivity of the subsurface material as a function of (Λ_m / Λ_s) optimum value; the computations correspond to the optimal condition $w = (2n + 1)\,\lambda_{ml}/4$ and $n = 15$. For the y-axis range, $\varepsilon_{ml} \in (1.0 – 10.0)$ corresponds to the subsurface layer thickness $w \in (35 – 120)$ meters for the typical SHARAD parameters and optimal conditions. The increase in ε_{ml} with $(\Lambda_m / \Lambda_s)_{opt}$ is physically a consequence of a decrease in the dielectric contrast of the surface – subsurface interface. Another way around, the effect also can be understood from the expression in Eq.4 by increasing denominator magnitude corresponding to optimal condition. The dependence of the optimum power reflectance decreases with an increase in the attenuation factor – this is consistent with the results shown in Figure 4. This figure also

suggests that the intense reflections may infer to the subsurface materials having (*i*) low dielectric permittivity (low-density) or (*ii*) low attenuation coefficient.

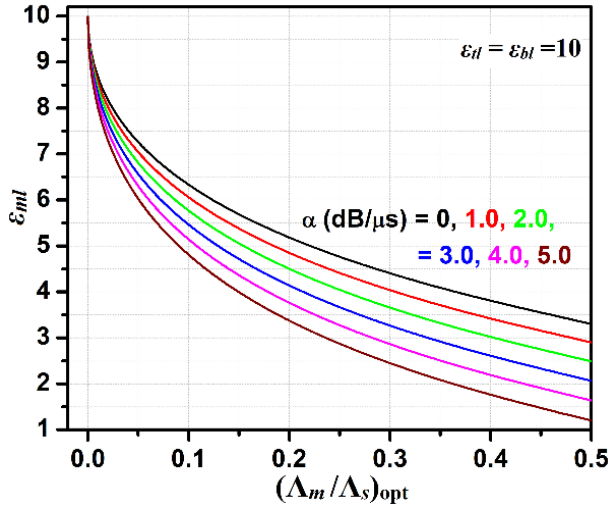

Figure 5: *Optimum value of the power reflectance* $(\Lambda_m / \Lambda_s)_{opt}$ *as a function of the subsurface dielectric permittivity* (ε_{ml}) *using Eq.*5 *for* $w = (2n + 1)\,\lambda_{ml}/4$, $n = 15$, $v = 20$ MHz *and* $\varepsilon_{tl} = \varepsilon_{bl} = 10.0$. *The colored lines refer to different values of α, as marked in the figure.*

Summary

In this article, we have briefly portrayed an overview of the concept and operation of the SHAllow RADar (SHARAD) onboard MRO spacecraft – the instrument is a powerful tool to analyze and understand the Mars geology, stratigraphy, and geographical evolution. We have discussed the SHARAD data analysis, graphical representation, and a plausible approach to determine the dielectric properties of the subsurface material. The analysis suggests that the subsurface reflections are the impression of dielectric properties of the subsurface material, and dielectric permittivity may be obtained using the sounding radar observations of the subsurface reflectivity. The specs of the SHARAD instrument make it appropriate to refine the stratigraphy for the first few 100 meters beneath the surface – SHARAD has demonstrated its significance by discovering the ice layers around polar caps [9], and in the northern and southern mid-latitude regions on Mars [14]. This instrument complements its companion instrument MARSIS, and both together are capable of providing unique insight about the Mars evolution. Based on the present understanding of the orbiter radars, multi-frequency operation of the instrument may be of significant means to complement the high penetration with better resolution in forthcoming projects – such sounding radars are capable of probing the icy moons of Jupiter/ Saturn and the cometary atmosphere.

Acknowledgments

The authors acknowledge the support from the Department of Space, Government of India, in accomplishing this work.

References

1. Spaceborne radar remote sensing: Applications and techniques by Elachi Charles (IEEE Press, NY, USA, 1988)
2. S. P. Kingsley et al., Adv. Space Res. **23**, 1929 (1999)
3. Radar Remote Sensing of Planetary Surfaces by Bruce A. Campbell (Cambridge, NY, USA, 2002)
4. E. Flamini et al., 4th International Workshop on Advanced Ground Penetrating Radar, Aula Magna Partenope, p. 246 (2007)
5. J. Mouginot et al., **39**, L02202 (2012)
6. R. Orosei et al., Science **361**, 490 (2018)
7. R. Seu et al., Planetary & Space Sci. **52**, 157 (2004)
8. R. Seu et al., Jour. Geophys. Res. **112**, E05S05 (2007)
9. N. E. Putzig et al., Icarus **204**, 4432 (2009)
10. C. M. Stuurman et al. **43**, 9484 (2016)
11. P. Choudhary et al., IEEE Geosci. & Rem. Sens. Lett. **13**, 1285 (2016)
12. I. B. Smith, & J. W. Holt, J. Geophys. Res. Planets, **120**, 362 (2015)
13. M. H. Carr, & G. G. Schaber, J. Geophys. Res., **82**, 4039 (1977)
14. Plaut et al., Geophys. Res. Lett. **36**, L02203 (2009)
15. G. Alberti et al., Jour. Geophys. Res. **117**, E09008 (2012)
16. Propagation of Electromagnetic Waves in Plasma by V. L. Ginzburg (Gordon & Breach Science, London, 1961)
17. Microwave dielectric spectrum of rocks by F. T. Ulabay et al. (Rep. 23817-1-T, Univ. of Mich. Radiat. Lab., Ann Arbor, 1988)
18. M. N. Simon et al., Jour. Geophys. Res.: Planets **119**, 2291 (2014)
19. L. M. Carter et al., Geophys. Res. Lett. **36**, L23204 (2009)
20. B. Campbell et al., Jour. Geophys. Res. **113**, E12010 (2008)